

Process Errors and Aspects for Higher Resolution in Conventional Stereolithography

Carsten Tille

caesar research center

Ludwig-Erhard-Allee 2, 53175 Bonn/Germany

1 Abstract

Due to the rapid development of precision manufacturing technologies, there is a growing market need for appropriate rapid prototyping methods with higher resolution. This paper presents aspects for a general optimization of stereolithography accuracy and gives a deeper analysis of important process errors.

Beside a higher precision due to improved optical components, it can be shown that for a better vertical resolution one must mainly reduce the penetration depth of the photopolymer. We found that this is also possible with conventional stereolithography materials by using a different wavelength, achieving cured rugged layers with a thickness of 20 micrometer.

The major accuracy aspect lies in the understanding of the layer deposition process. A CFD (computational fluid dynamics) study helps to describe important phenomena of blade based coating techniques. As a result, the inaccuracy of the layer deposition is the general limiting factor in stereolithography.

This knowledge can be directly applied to commercial stereolithography systems helping users to achieve higher process accuracy.

2 Introduction

Stereolithography (SL) is the best-known rapid prototyping process and widely used as a tool for product development. A strong goal for a further improvement of the SL process is on higher quality of stereolithography parts with simultaneous consideration of cost and practical feasibility. For this reason, one must in particular analyze and assess the influence of stereolithography process itself on the part quality. As is known, stereolithography uses an UV laser for a layer-wise polymerization of selected areas of a liquid photosensitive resin. Three major sources for a negative influence on the part quality can be identified and have to be analyzed separately:

- UV exposure of the photopolymer,
- Polymerization behavior,
- Layer application (recoating).

A number of different authors have done basic work on the investigation of those problems. This paper can only concentrate on some special problems of the stereolithography principle itself, and it tries to add some new aspects for the improvement of the stereolithography part accuracy. Any kind of material behavior, which is based on shrinkage effects, has been deliberately excluded although it is known that this can also have strong influence on the quality of parts.

For this research on process errors different stereolithography apparatuses were examined: an older EOS Stereos Desktop, a new 3D Systems Viper Si² and the MSTL, a flexible research system, mainly used to investigate the influence of single process parameters. The latter test platform has the ability to work with a focal diameter from 16 to 100 microns and a layer thickness from 20 to 100 microns.

3 Influence of the optical unit and polymerization

3.1 Optical unit

The function of the optical unit is the correct illumination of the resin surface. The beam diameter has direct influence on the area that is to be cured. Therefore, any beam forming optical component has to be examined carefully. A first step for a higher process resolution is usually the increase of the beam quality of the UV laser [JAC92]. Today HeCd or solid-state systems are available with a beam mode quality close to the ideal Gaussian beam profile of $M^2 \approx 1$. The beam pointing, in particular for HeCd lasers, should be low to ensure a stable position of the beam on the resin surface. Furthermore, it is possible to design and manufacture important optical components like the beam expander as diffraction-limited systems. Due to the hyperbolic shape of the propagating beam, any deflection of the galvanometer scanners leads to a suboptimal beam diameter on the resin surface. While a larger distance between scanner unit and resin can help to reduce this effect, only a flat-field lens like an f-T system or a dynamic focusing unit can assure an optimal beam diameter across the whole build envelope. The described optimizations were carried out and lead to optical results shown in table 1 [TIL03]:

	Focal length of f-T lens	Beam diameter $2w_0$ (13,5%)	Effective working envelope
MSTL test system	$f_{f-T} = 220$ mm	$16 \mu\text{m} \pm$ approx. 20%	$\varnothing 100$ mm
EOS Stereos Desktop	$f_{f-T} = 500$ mm	$50 \mu\text{m} \pm$ approx. 20%	250x250 mm
Reference: [3D Viper]	-	$80 \mu\text{m} \pm$ approx. 20% [HR]	100x100 mm [HR]

Table 1: Optical parameters for different optimized stereolithography systems

The negative effect of the galvo scanner and the (optional) f-T lens on the geometric distortion of the scanned image is usually corrected by means of a software-based compensation. A pre-calculation of the distortion matrix using ray-tracing software turned out to be an effective way to avoid inaccuracy in measuring exact laser spot positions. This procedure is recommended in particular for higher resolution stereolithography systems. For the described high-resolution test system, an integrated real-time position correction with accuracy better than $\Delta x < 1 \mu\text{m}$ could be demonstrated [TIL03].

The last optional component, the acousto-optical modulator is used to blind out dynamic effects on the spot motion due to the inertia of the scanning mirrors. Again a correction of dynamic errors was shown for the high-resolution MSTL system with a total accuracy better than the spot radius $w_0 = 8 \mu\text{m}$ [TIL03]. Parallel to this measure, variable beam expanders are able to deliver two or more different beam diameters on the resin that allow to work with higher laser power and reduced total exposure time [DEU99].

3.2 Problems of polymerization

Polymerization problems play – in addition to the optimization of laser spot – an important role for the aim of higher process resolution. As a precondition, the laser light must homogeneously illuminate the layer in order to achieve an equal layer thickness and thus a good part quality. This is typically achieved by a sufficient overlap of the hatch lines [JAC92]. In the transition region from hatch to contour lines, the non-homogenous exposure leads to a variable degree of polymerization and thus higher wall roughness. Other influencing parameters are the non-perpendicular direction of the deflected beam to the resin surface, the energy distribution using variable spot diameters (contour and hatch) or the over-exposure problem [JAC92, TIL03].

The cure depth C_d of the photopolymer is important for the vertical resolution of the stereolithography process. A reduced energy density E on the resin surface allows the reduction of C_d but reduces also the green part strength. This behavior can be explained by the model of the photo modulus Y [JAC92]

$$\frac{Y}{Y_{\max}} = 1 - e^{-\beta \left(\frac{E}{E_c} - 1 \right)} \quad \text{with} \quad \beta = \frac{K_p E_c}{Y_{\max}}, \quad (1.1)$$

where Y describes the Young's modulus depending on the exposure energy density E . A solution for this problem is found in a better absorption that leads to higher degree of polymerization and thus to a higher Young's modulus. The absorption a of a resin can be changed by the parameters concentration c or extinction ϵ , where the relation to the well-known penetration depth D_p is

$$D_p = \frac{1}{a} = \frac{1}{\epsilon \cdot c} \quad (1.2)$$

For commercial polymers, it is only possible to take advantage of the dependency of extinction ϵ from the wavelength λ . A change in the exposure wavelength can then result in a new penetration depth D_p . This relative change α_A of the absorption is then described as:

$$\alpha_A := \frac{a(\lambda_1)}{a(\lambda_2)} = \prod \frac{c_i(\lambda_1) \epsilon_i(\lambda_1)}{c_i(\lambda_2) \epsilon_i(\lambda_2)} \xrightarrow{c_i = \text{const.}} \alpha_A = \frac{\epsilon_{\text{total}}(\lambda_1)}{\epsilon_{\text{total}}(\lambda_2)} = \frac{D_p(\lambda_2)}{D_p(\lambda_1)} \quad (1.3)$$

The absorption was investigated for different commercial resins using a HPLC with a TPM dilution of 1:1500. All assayed resins are designed for a wavelength of $\lambda_2 = 355$ nm (frequency-tripled solid state laser). The results presented in figure 1 show a considerable dependency of the absorption on the wavelength. Looking at $\lambda_1 = 325$ nm (HeCd laser), one can find for all resins (acrylate, epoxy) a reduced penetration depth, resulting in a relative change from $\alpha_A = 2,5..14,5$.

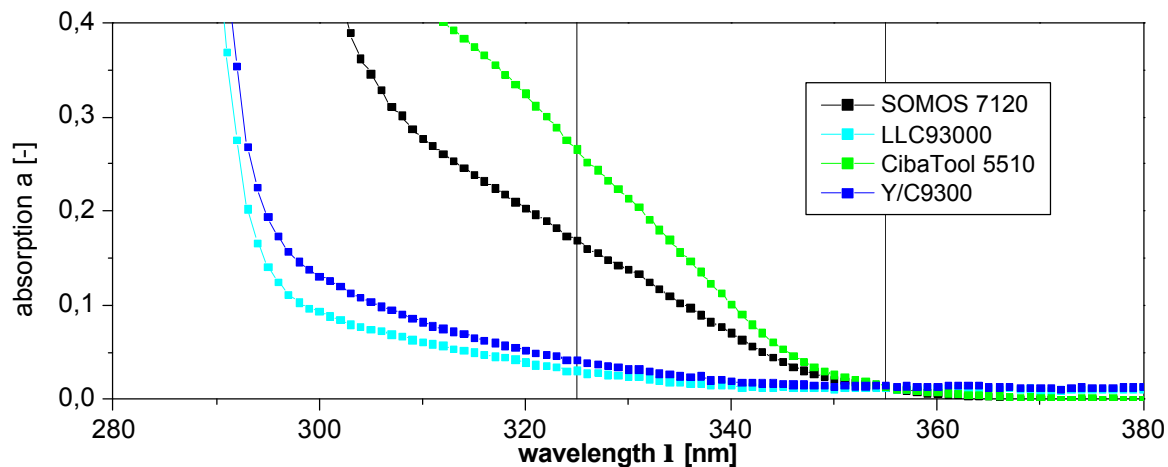


Figure 1: Absorption characteristics of different commercial resins (TPM dilution 1:1500)

This result can be compared to the measured cure depth of a resin exposed with a differing wavelength. For that purpose, one single resin (SOMOS 7120) was investigated using a Liconix HeCd M3-14 laser and the windowpane method [JAC92, www.dsmsomos.com].

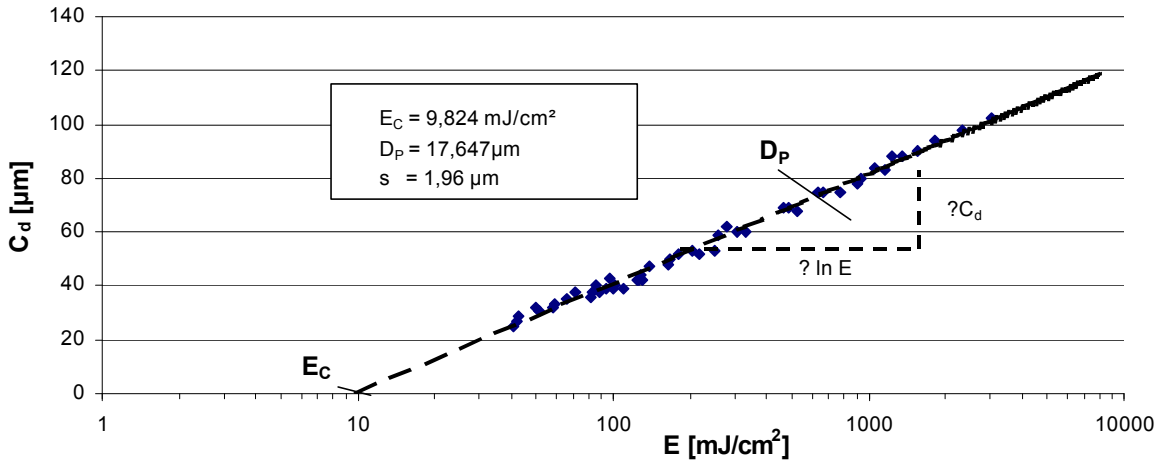


Figure 2: Working curve for SOMOS 7120 at $\lambda_1 = 325 \text{ nm}$ (HeCd laser, MSTL test system)

The resulting penetration depth $D_p = 17,6 \mu\text{m}$ obtained from the analysis of the thickness of the windows (fig. 2) proves the idea of the absorption measurement (1.3) that predicts a comparable penetration depth:

$$D_{p,325 \text{ nm}} = \frac{D_{p,355 \text{ nm}}}{\alpha_A} = \frac{140 \mu\text{m}}{9,8} = 14,3 \mu\text{m} \quad (1.4)$$

To sum up this section, it could be clearly shown that a multitude of measures is available to improve the resolution and accuracy of a stereolithography part by optimizing the laser exposure and polymerization characteristics.

4 Layer Application Problems

4.1 Introduction to recoating

Beside process errors caused by the irradiation of the resin, a second source of inaccuracy is found in the layer application or recoating systems. Conventional stereolithography uses recoating systems based on the transportation of liquid resin onto the surface of a previously cured layer. Although there exist different systems, they all have in common that liquid is scraped from the vat with a certain resin level onto a dry surface.¹

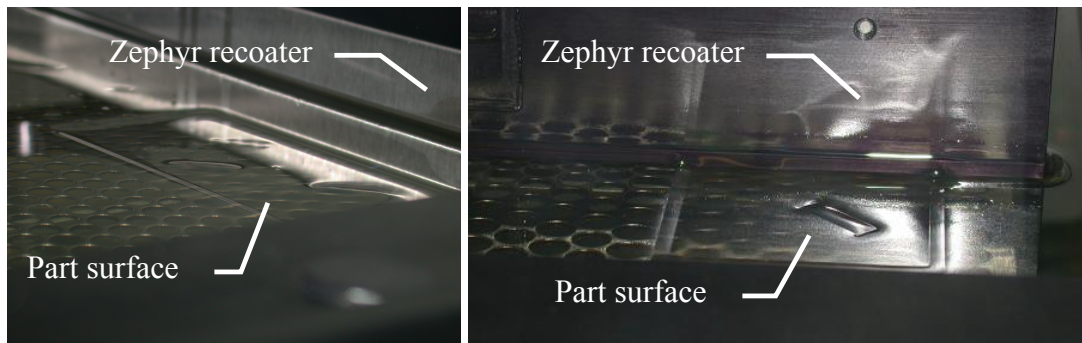


Figure 3: Faulty, uneven surface after recoating (le.) and exposure (re.) on a Viper Si² stereolithography system

¹ An exception is the so-called deep-dip principle and is only of limited relevance for today's stereolithography apparatuses. This method will be discussed as a secondary case.

It is known that all recoating systems can cause significant inaccuracy in the vertical (z-)direction of the part, figure 3. The aim of the following section is an in-depth analysis of recoating errors by means of computational fluid dynamics simulations. Figure 4 schematically illustrates typical recoating errors, whereas the main errors can be classified in two groups:

- Layer thickness error
 - Dewetting
 - Peak
 - Part height error
 - Closed volume error (C/V)
 - Delamination
- } related to a single layer
- } related to a sequence of layers

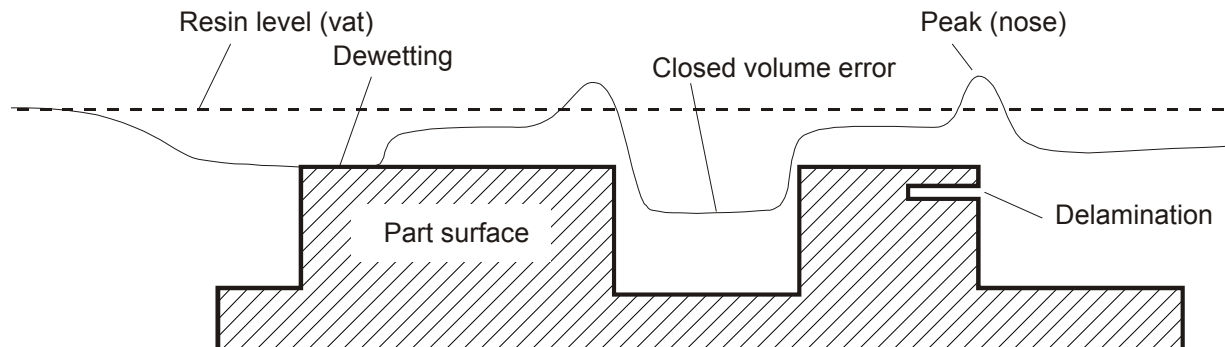


Figure 4: Designation of typical recoating errors

4.2 CFD-Simulation for blade recoating system

In contrast to earlier investigations, this study is interested in understanding more details of the layer application principles [REN95]. For this we used the numerical fluid simulation software Flow3D because of its outstanding capability to simulate surface tension problems together with moving objects. The software gives transient solutions of mass and impulse equations on an orthogonal finite volume grid. All objects are specified with the help of the FAVOR algorithm (cell volume parts). Free surfaces are described by the Volume-of-Fluid technique (VOF) and surface tension effects are included [HIR81, HIR98].

The simulation model consists of a two-dimensional grid laid in the main recoating direction, figure 5. The problem is modeled assuming a Newtonian liquid and laminar, incompressible flow. To investigate over longer time, the reference system was coupled to the recoating system. The part is moving with (negative) recoating speed u_{RC} . Inflow and outflow are simulated as constant velocity respectively zero-gradient condition. The simulations use different grid sizes from 150×75 cells up to 600×200 cells for larger problems. The sub-grid accuracy of the VOF algorithm allows, despite the number of cells, an exact determination of the height of the resin surface.

The introduced simulation parameters varied due to the nature of the problem that was simulated in each case. Generally, a model resin was used according to specific values taken from the data sheet of SOMOS7120 from DSM [www.dsmsomos.com]. The recoating speed ranges from $u_{RC} = 2$ to 50 mm/s. The recoater material simulates standard stainless steel; the shape of the blade is rectangular with the width b_A .

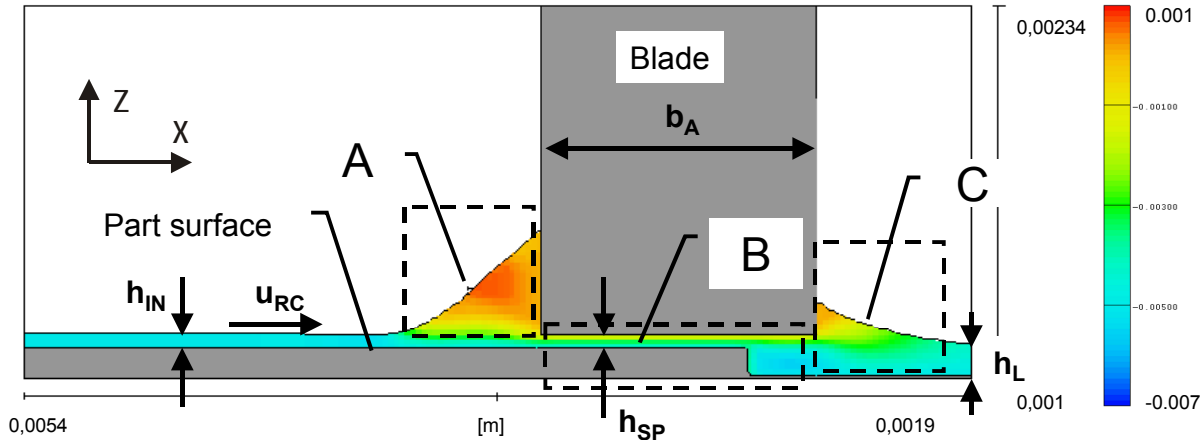


Figure 5: CFD model of resin with moving blade resp. part with three flow regions (colored: velocity component in x , $u_{RC} = 5 \text{ mm/s}$, $b_A = 1 \text{ mm}$, SOMOS 7120, step $h_{SP} = 50/150 \text{ } \mu\text{m}$, $t = 0,35 \text{ s}$)

Three major characteristic flow regions can be identified (figure 5):

- A (bow wave): Inflow in A creates a bow wave in front of the blade. Shear and gravity forces rapidly dominate in this region in comparison to capillary forces.
- B (gap current beneath the blade): The flow is simplified as parallel laminar flow. For very large gaps, the flow changes its character.
- C (stern wave): The resin forms a stern wave at the rear side of the blade. This wave is in balance with capillary and friction forces.

The situation found in region A and B confirms the general idea of earlier research work [REN95]. However, important recoating problems could not be explained in detail. In this situation, the CFD simulation can help to understand the underlying basic elements of the recoating process.

Looking at region B, the flow beneath the blade is estimated as a parallel flow. With an assumed pressure gradient P over the gap the flow can be described with as a Couette-Poiseuille flow $u(z)$ with a parabolic flow profile:

$$u(z) = u_{RC} - \frac{z}{h_{SP}} \left(u_{RC} - \left(1 - \frac{z}{h_{SP}} \right) \frac{P h_{SP}^2}{2 \eta} \right) \quad \text{for } h_{SP} \leq h_{SP,CP} \quad (1.5)$$

This theory is obviously true only for small gaps h_{SP} between recoating blade and part surface. Because one would expect also an influence of the blade width b_A , the aspect ratio b_A/h_{SP} is defined as a more precise condition. For small aspect ratios, one expects a transition to an unchanged flow comparable to a flow onto a flat plate. With this very simple assumption the outer flow – which exists apart from the blade and stays unchanged – can be described with the displacement thickness $d_1(x)$. Here d_1 is a measure for the displace effect of the boundary layer:

$$\delta_1(x) = \frac{1,7208 x}{\sqrt{Re_x}} = 1,7208 \sqrt{\frac{\nu x}{u_{RC}}} \quad \rightarrow \quad h_{SP} \leq h_{SP,CP} = 1,7208 \sqrt{\frac{\nu b_A}{u_{RC}}} \quad (1.6)$$

From equation (1.6) can be followed that a Couette-Poiseuille flow can only develop if $h_{SP} = h_{SP,CP}$, where x is set to the blade width b_A and the displacement thickness is simply expected to fill the gap at least at the end of the blade gap. If there are larger gaps with $h_{SP} > h_{SP,CP}$ one would find an unchanged flow field beyond the boundary layer and no flow resistance.

Sample simulations for different geometries ($b_A/h_{SP} = 1:0,5$ to 100) and recoating parameters were carried out to prove the described concept. The results showed a sufficient agreement with the Couette-Poiseuille flow $u(z)$ for arbitrary pressure gradients from $P = 0$ to 7200 Pa/m.

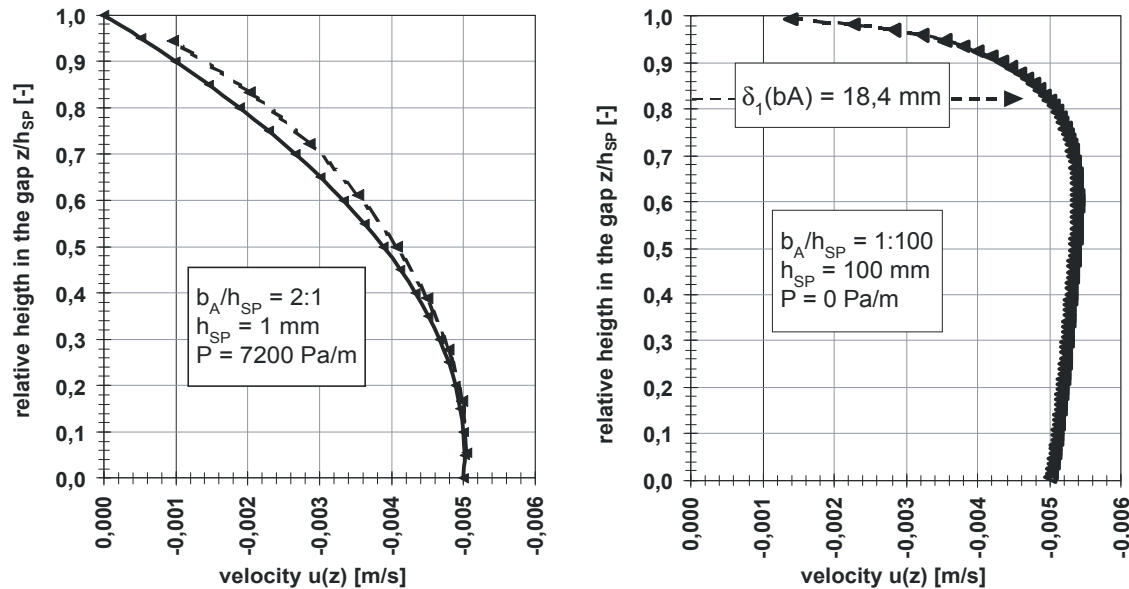


Figure 6: Sample CFD flow profiles in a gap for different gap heights h_{SP} (- - -, velocity component in x) (left: compared to Couette-Poiseuille profile (—), standardized height z/h_{SP} , $u_{RC} = 5$ mm/s, SOMOS 7120)

For ratios of b_A/h_{SP} up to approximately 1:10 only small deviations to the Couette-Poiseuille flow can be detected. Beyond this ratio, the displacement thickness d_1 gives a good approximation where the boundary flow changes to an unaffected outer flow (according to resting fluid).

Looking at the velocity profile in the gap, one can reason that in the case of a simple Couette flow ((1.5) with $P = 0$) not all resin can pass the gap; a bow wave can arise. As soon as the bow wave grows, a pressure gradient P develops over the blade. The (very small) hydrostatic pressure can – if we following the idea of [REN95] – cause an increased flow rate into the deposited layer.

As a precondition, the recoater needs a certain amount of resin that has to be transferred for the generation of a layer. This resin – described as inflow in the simulation – can be taken from resin moved by the blade itself due to surface tension, it can be deposited by an active recoating system or it can remain from a previous deep-dip operation. In general, the inflow must not be smaller than the outflow, otherwise the fluid flow will stop and dewetting occurs. If there is enough inflow h_{IN} and friction forces exist (Couette-Poiseuille flow), a bow wave is inevitably piled up in front of the blade. Thus, a pressure gradient P across the blade develops because of the hydrostatic pressure in the bow wave. For a larger bow wave or greater gap height, there is an imbalance and the bow wave can leak through the gap. This effect leads to an increasing layer thickness h_L . In this case, layer thickness is larger as expected from a plain Couette flow ($h_L = h_{SP}/2$). As already said, this consideration is only valid if there is sufficient friction in the gap. It can be expected, that if the gap height exceeds the displacements thickness ($h_{SP} > h_{SP,CP}$), no bow wave can develop.

For small gaps – typically found on the surface of a part – the bow wave increases very fast if there is enough resin inflow to the recoater ($h_{IN} > h_{SP}/2$). The hydrostatic pressure in the bow wave leads to a compensating flow in direction of the movement of the recoater. This results in a

decreasing height and increasing length of the bow wave and thus smaller P. The simulation shows slow balancing through the domination gravity g and viscosity η , figure 7.

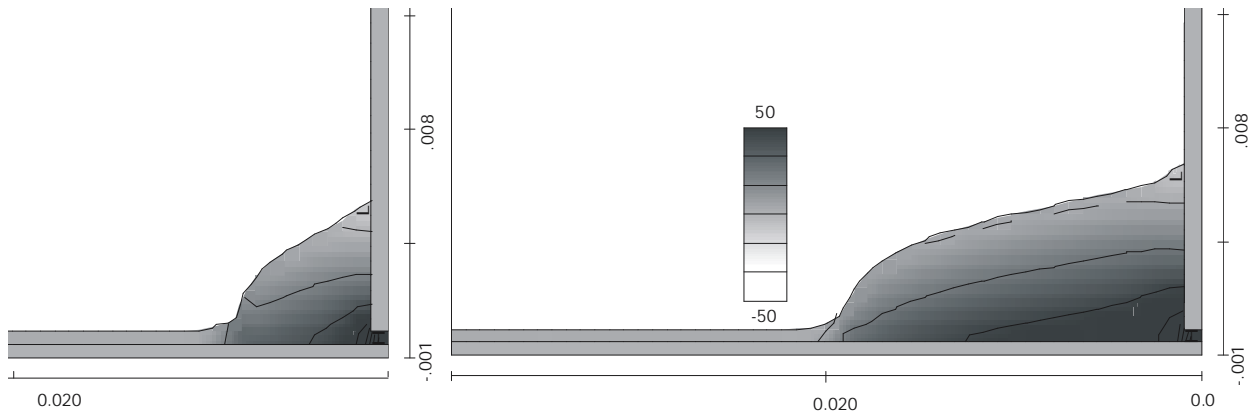


Figure 7: Typical profile and pressure distribution (p [Pa]) of a larger bow wave at two different times $t_1 = 3$ s (le.) $< t_2 = 8$ s (re.) (SOMOS 7120, $u_{RC} = 20$ mm/s, $b_A = 5$ mm, $h_{SP} = 250$ μ m, length units[m])

The simulation shows a surface with negative curvature behind the blade, comparable to a stern wave. This curvature of the resin surface correlates with a negative pressure difference Δp_{HW} to the inside of the wave, what can be followed from the Young-Laplace-Equation:

$$\Delta p_{HW} = p_{HW} - p_0 = \frac{\sigma_s}{R} < 0 \quad (1.7)$$

This capillary pressure difference must be in balance with viscosity forces for constant process conditions and thus results in an extended pressure gradient P across the blade. It can be concluded from the simulation that the pressure gradient P will be dominated for small gaps h_{SP} by the stern wave and for larger gaps ($> h_{SP,CP}$) by the bow wave. This assumption was confirmed with a series of CFD simulations, figure 8.

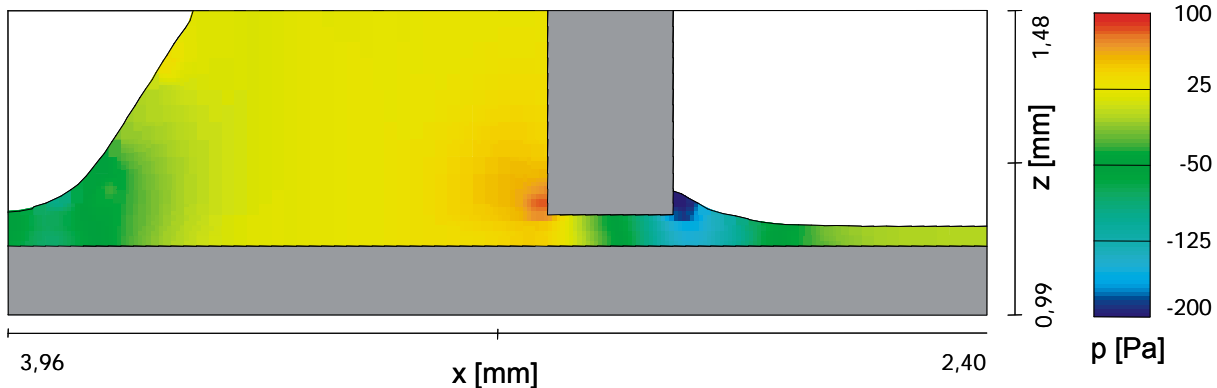


Figure 8: Typical pressure distribution due to bow and stern wave for a low recoating speed ($u_{RC} = 5$ mm/s, $h_{SP} = 150$ μ m, $b_A = 1$ mm, $t = 2,8$ s, $h_{IN} = h_{SP}$, SOMOS 7120)

Moreover, from the simulations one can follow, that for simple recoating systems (blade) in some situations a small amount of additional resin is deposited at the front side of the part. The amount of resin is referred to as peak or nose and can always be found at the beginning of a step, i.e. at the transition from larger to small gap h_{SP} beneath the blade. An examination of results from the CFD simulation (figure 9) suggests an explanation for this effect: The blade moves a reasonable amount of resin as part of the volume of the stern wave onto the surface of the part. Then a peak develops as a leakage of the stern wave caused by the friction suddenly occurring on top of the part. Because the stern wave can mainly be described as a free or viscous meniscus,

the peak is minimized by reducing the volume of fluid transported at the back of the blade. A change of the contact angle between resin and blade or an optimized blade profile represent simple solutions.

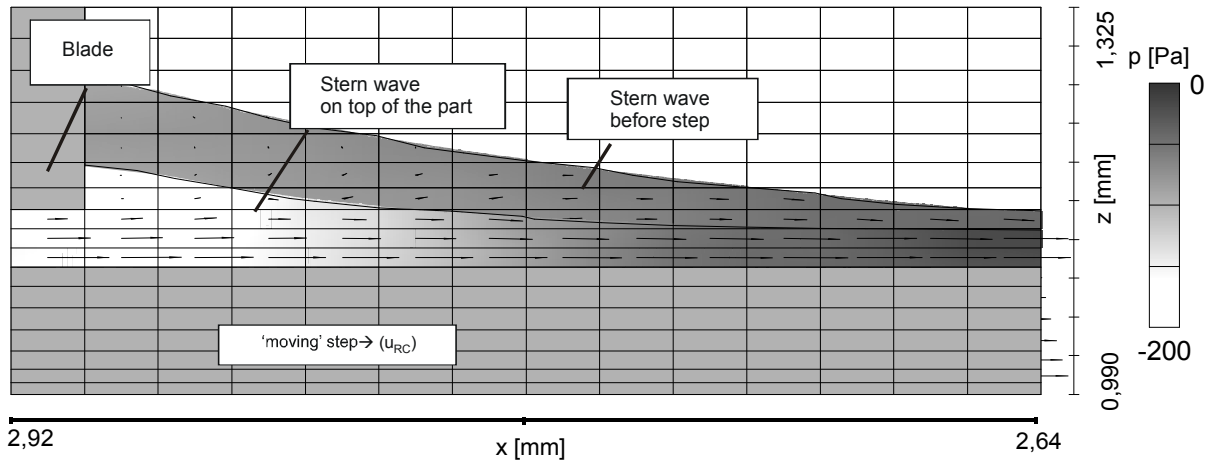


Figure 9: Leakage of the stern wave – comparison of surface profile and pressure distribution before and on a part (SOMOS 7120, $u_{RC} = 5\text{ mm/s}$, $b_A = 1\text{ mm}$, $h_{SP,1} = 5000\text{ }\mu\text{m}$, $h_{SP,2} = 150\text{ }\mu\text{m}$)

The previous simulations depict only two-dimensional situations of the recoating problem. A flow perpendicular to the simulation plan may be important as soon as there are part geometry changes in this direction. This is of course the case in the majority of situations. Because a three-dimensional problem increases the computational effort, one simple three-dimensional structure consisting of a step on the top of a first step with a conjoint sloping sidewall parallel to the previous two-dimensional calculation plane was examined, figure 10. The simulation shows that there is only very limited flow parallel to the steps (i.e. y-direction, perpendicular to the former calculation plan). From this result and practical experience one can follow that only near significant geometry changes the two-dimensional flow regime is disturbed noticeably. As a scale for the distance of the disturbed area, one can use the gap height h_{SP} .

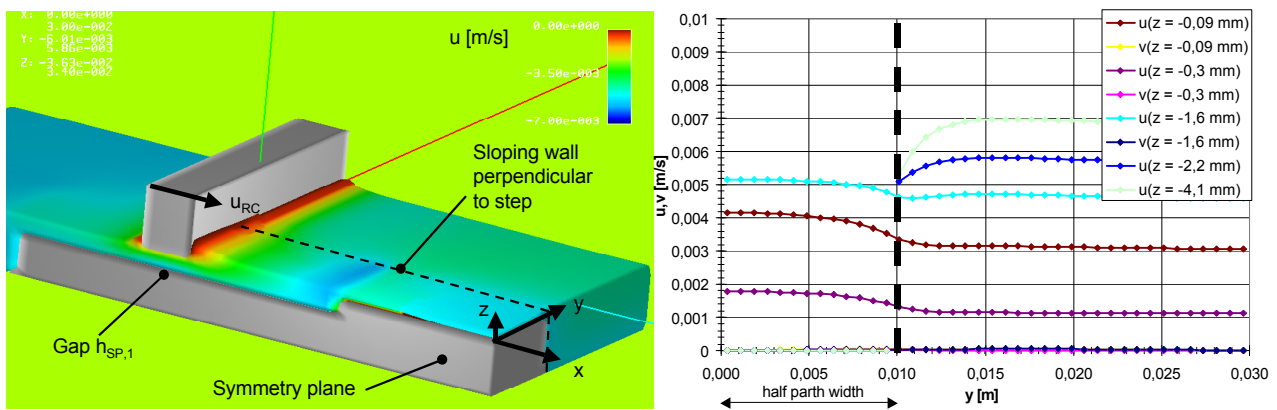


Figure 10: 3D model (half-section) of a blade on a double step and lateral wall (le.); (re.) typical effect near the sloping wall on the forward velocity component u and transversal velocity component v beneath the blade for different depth z (SOMOS 7120, $u_{RC} = 5\text{ mm/s}$, $h_{SP,1} = 1,9\text{ mm}$, $h_{SP,ground} = 5\text{ mm}$, $b_A = 5\text{ mm}$)

4.3 Experimental data

Selected simulation results were checked by profile measurements of the resin surface. Regrettably, it is not possible to evaluate the flow distribution and the surface profile directly on every point near the recoater with standard equipment. However, the height of the resin behind

the blade was determined using a laser triangulation sensor (MikroEpsilon ILD2000). The sensor was tilted over half the angle between the laser beam and the reflected beam to achieve a better signal. The height h_L of the layer on the surface of a flat artificial part (polished PMMA) was measured after SOMOS 7120 resin was spread previously and recoated by a simple blade. The measuring point was chosen in sufficient distance to any peak phenomenon. The measurement values for different recoating speeds u_{RC} and gap heights h_{SP} are compared to the simulation results in figure 6. It has to be remembered at this point that h_L can vary between $h_{SP}/2 < h_L < h_{IN}$. The error of the layer thickness h_L can differ from the intended resin level significantly; depending on part geometry this might exceed the (geometrical) slice thickness several times.

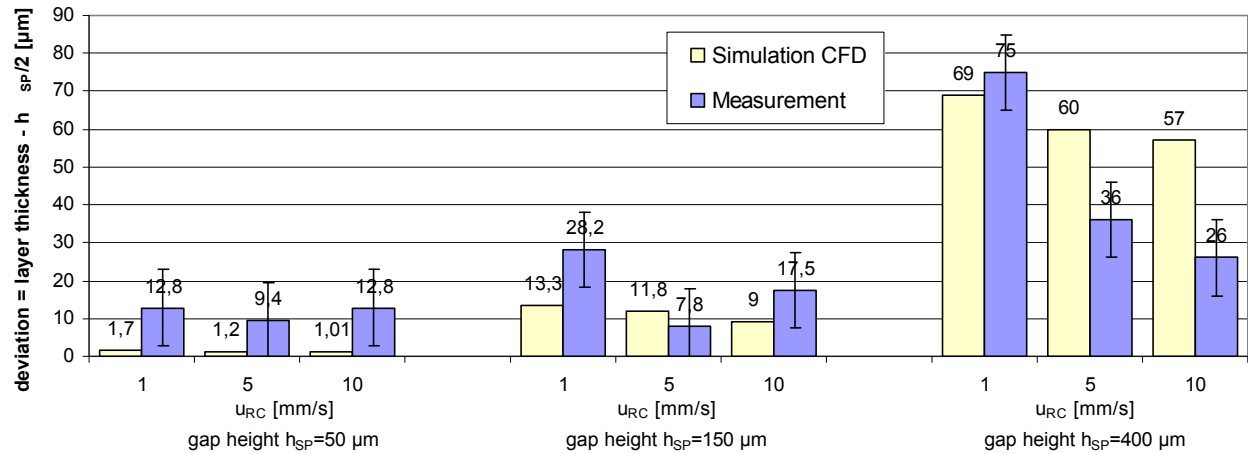


Figure 11: Abs. deviation of layer thickness h_L comp. to $h_{SP}/2$ under different recoating conditions (SOMOS 7120)

4.4 Related recoating systems

The blade recoater provides a basis for understanding more complex recoating system. The active recoating used by many SLA's from EOS can deposit a constant volume flow in front of a blade.² The pump causes an additional constant inflow towards the blade and can therefore be regarded as a blade system with (additional) inflow h_{IN} .

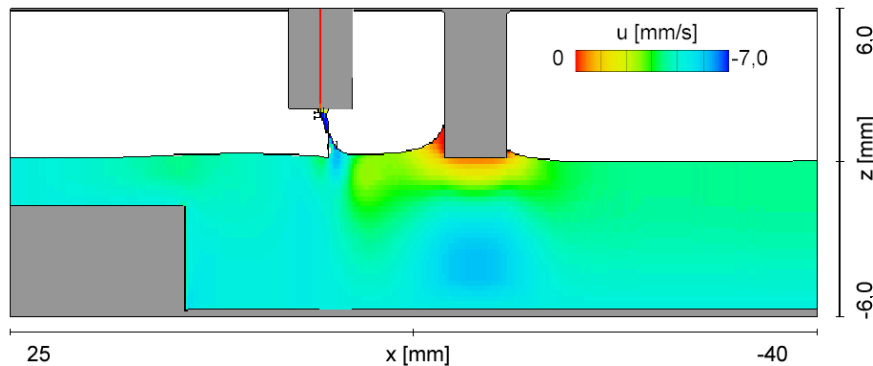


Figure 12: Semi-curtain effect and velocity profile (velocity component u in x) of a active recoating system moving towards a large step (SOMOS 7120, $b_A = 5 \text{ mm}$, $u_{RC} = 5 \text{ mm/s}$, volume flow for a $400 \mu\text{m}$ layer, $t = 0,8 \text{ s}$)

The low pressure recoating³ used in 3D-Systems's SLA is a more complex system in terms of the flow characteristics. The chamber – limited by two walls – can transport additional resin onto the

² The second (or ,first') blade in those systems can be interpreted as a simple blade system as described before.

³ Zephyr®

surface of the part. While for larger gaps beneath the recoater the simulations shows nearly no flow in the chamber one can find a small circular flow due to the increased friction when the recoater moves on the surface of the part. Again, a small bow wave develops if a previous resin layer exists (deep dip).

In general, one can follow that the basic characteristics of those recoating systems are to some extent comparable to the simple blade principle due to the similar parallel flow regime beneath those structures.

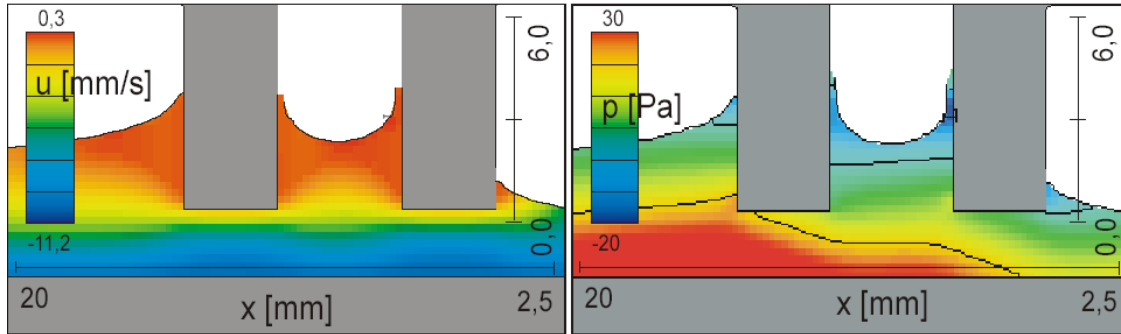


Figure 13: Low pressure recoater – velocity (component u in x , le.) and pressure (re.) distribution ($u_{RC} = 10$ mm/s, SOMOS 7120, $h_{SP} = 400$ μ m, $b_A = 3$ mm each)

4.5 Influence of recoating errors on part geometry

Every error in the recoating process leads consequently to a geometric deviation of the part since the laser exposure cures the existing resin surface. Recoating errors can deviate strongly from the aimed layer thickness and can reach a multiple of the geometrical slice thickness since they depend mainly on the gap between blade and part surface (see 4.2). Only larger errors of more than approx. 1 mm will lead to a slow compensation flow due to gravity effects [TIL03]. Sequential application of resin with any recoating method introduces larger errors of the z -height of the part. Those errors are caused by the variable layer thickness applied by the recoater and depend on whether the area is connected to surrounding resin or not (closed-volume effect). Regrettably, a full CFD simulation of a complete part building process is currently beyond the possibilities of even recent personal computers.

5 Discussion

The paper analyses specific process errors of the stereolithography. Solutions for reducing particular exposure or recoating based process errors can be given based on the described investigations. Generally, a reduction of stereolithographic process errors can be achieved by the following steps:

- Exposure: Beside the installation of a laser with Gaussian beam profile an optical upgrade kit with f-T lens can increase the resolution. Considerably more difficult is the optimization of the scanner control, while a reduced scanning speed (and laser power) will generally increase the positioning accuracy.
- Polymerization: A reduced cure depth C_d (together with a sufficient stiffness) can be achieved by higher absorption. This is also possible for many commercial photopolymers if a laser with shorter wavelength is utilized.
- Recoating: All commercial recoating systems generate large errors in the part geometry that cannot be eliminated. Only limited optimization is possible due to the nature of the

friction-driven flow beneath the recoater. This flow leads to a variation of the height of the applied layer depending on the gap height and other parameters. Low viscosity and low recoating speed can help to minimize the gap height range up to that friction forces influence the flow.

Constant recoating conditions are possible if an (irregular) part geometry is surrounded by a flat support grid structure, figure 14. This grid structure may increase the process time significantly but produces a steady recoating error that might be corrected by means of software. A grid support is sometimes the only approach for the precise manufacturing of very small parts.

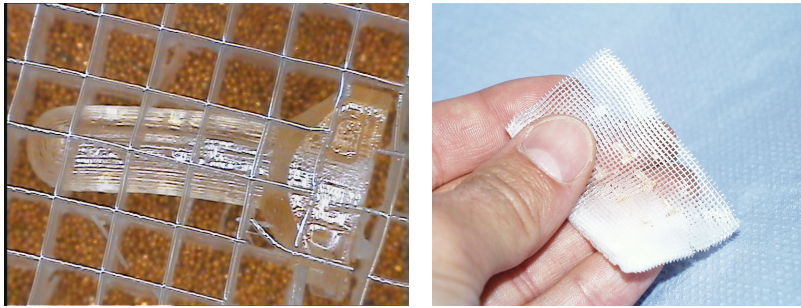


Figure 14: A grid based support structure helps to achieve constant recoating conditions and protects small parts

6 Conclusion

Stereolithography remains the standard process with the potentially highest resolution and - to some extent - accuracy compared to other commercial available processes like powder based or even polymer-jetting principles.

The optical unit can be optimized to a very high degree but recoating remains the largest problem. Knowing the influence of system based process errors in stereolithography can help to optimize processes and might be a starting point to further improvements. As an outlook, an integrated software correction based on an analytical recoating model can help minimize the recoating errors by means of a local pre-deformation of the part geometry.

7 Acknowledgement

Grateful acknowledgement is made to the Bayerische Forschungsstiftung (Munich) and caesar (Bonn) for their support of this work. I would like to especially thank Prof. Heinzl of Technical University Munich and his students for the prolific collaboration.

8 References

- [DEU99] Deuke, R., Tille, C., Eidam, R.: New Lasers in Stereolithography - pushing abilities to the limit. uRapid '99. London, 1999, 43-53
- [HIR81] Hirt, C.W.; Nichols, B.D.: Volume of Fluid (VOF) Method for the Dynamics of Free Boundaries. Journal of Computational Physics 39 (1981) 201-225
- [HIR98] Hirt, C.W.; Choinski, E.: Simulation of the Wet-Start Process in Slot Coating. In: Proc. 9th Int. Coating Science & Technology Symposium, Newark, May 18-20, 1998
- [JAC92] Jacobs, P.F.: Rapid Prototyping and Manufacturing: Fundamentals of Stereolithography. Dearborn: Society of Manufacturing Engineers, 1992
- [MAR91] Marshall, G.F.: Optical Scanning. New York, Basel: Marcel Dekker, 1991
- [PAR96] Partanen, J.P.: Enhanced resolution of stereolithography. In: Proc. of SPIE: Rapid Product Development Technologies, 1996
- [REN95] Renap, K.; Kruth, J.P.: Recoating issues in stereolithography. Rapid Prototyping Journal 1 (1995) 4-16
- [TIL03] Tille, C.: Probleme und Grenzen der Stereolithographie als Verfahren zur schnellen Herstellung genauer Prototypen. Technische Universität München, 2003